

Surface deformation associated with the March 1996 earthquake swarm at Akutan Island, Alaska, revealed by C-band ERS and L-band JERS radar interferometry

Zhong Lu, Charles Wicks, Jr., Ohig Kwoun, John A. Power, and Daniel Dzurisin

Abstract. In March 1996, an intense earthquake swarm beneath Akutan Island, Alaska, was accompanied by extensive ground cracking but no eruption of Akutan volcano. Radar interferograms produced from L-band JERS-1 and C-band ERS-1/2 images show uplift associated with the swarm by as much as 60 cm on the western part of the island. The JERS-1 interferogram has greater coherence, especially in areas with loose surface material or thick vegetation. It also shows subsidence of similar magnitude on the eastern part of the island and displacements along faults reactivated during the swarm. The axis of uplift and subsidence strikes about N70°W, which is roughly parallel to a zone of fresh cracks on the northwest flank of the volcano, to normal faults that cut the island and to the inferred maximum compressive stress direction. A common feature of models that fit the deformation is the emplacement of a shallow dike along this trend beneath the northwest flank of the volcano. Both before and after the swarm, the northwest flank was uplifted 5–20 mm/year relative to the southwest flank, probably by magma intrusion. The zone of fresh cracks subsided about 20 mm during 1996–1997 and at lesser rates thereafter, possibly because of cooling and degassing of the intrusion.

Résumé. En mars 1996, un essaim de séisme intense enregistré sous l'île d'Akutan, en Alaska, était accompagné d'un épisode de fissuration à grande échelle du sol mais sans provoquer l'éruption du volcan Akutan. Des interférogrammes radar produits à partir d'images JERS-1 en bande L et ERS-1/2 en bande C indiquent un mouvement de soulèvement associé à cet événement équivalent à plus de 60 cm sur la portion ouest de l'île. L'interférogramme JERS-1 montre une plus grande cohérence, spécialement dans les zones de matériaux de surface non consolidés ou de végétation dense. Il montre également une subsidence d'une amplitude similaire dans la portion est de l'île et des déplacements le long des failles réactivées au cours l'événement. L'axe de soulèvement et de subsidence se situe à environ N70°W, soit parallèlement en gros avec une zone de fissures récentes sur le flanc nord-ouest du volcan, aux failles régulières qui entrecoupent l'île et à la direction de stress maximum de compression dérivée. Une caractéristique commune des modèles qui est conforme à cette déformation est l'emplacement d'une dyke peu profonde dans le sens de la tendance sous le flanc nord-ouest du volcan. Avant et après l'événement, le flanc nord-ouest s'est surélevé de 5–20 mm/année par rapport au flanc sud-ouest, probablement suite à l'intrusion de magma. La zone de fissures récentes a enregistré une subsidence d'environ 20 mm durant la période 1996–1997 puis d'une intensité moindre par après, possiblement dû au refroidissement et au dégazage de l'intrusion.

[Traduit par la Rédaction]

Introduction

Interferometric synthetic aperture radar (InSAR) combines phase information from two or more synthetic aperture radar (SAR) images of the same area acquired from similar vantage points at different times to produce an interferogram. The interferogram, depicting range changes between the SAR and the ground, can be further processed with a digital elevation model (DEM) to image ground deformation at a horizontal resolution of tens of metres over areas of ~100 km × 100 km with centimetre to subcentimetre precision under favorable conditions (Massonnet and Feigl, 1998; Rosen et al., 2000).

Most volcanic eruptions are preceded by measurable ground deformation caused by pressurization of a magma reservoir or by upward intrusion of magma. The sense of ground movement often reverses from uplift to subsidence as the reservoir pressure decreases during the eruption, then reverses again when the reservoir starts to repressurize (e.g., Dvorak and

Dzurisin, 1997; Dzurisin, 2003). Surface deformation patterns can provide important insights into the structure, plumbing, and state of restless volcanoes (e.g., Dzurisin, 2003). Since the first successful application of InSAR to an active volcano, exploring

Received 27 April 2004. Accepted 24 August 2004.

Z. Lu¹ and O. Kwoun. Science Applications International Corporation (SAIC), National Center for Earth Resources Observation and Science (EROS), US Geological Survey, Sioux Falls, SD 57198, USA.

C. Wicks, Jr. US Geological Survey, 345 Middlefield Road, MS 977, Menlo Park, CA 94025-3591, USA.

J.A. Power. Alaska Volcano Observatory, US Geological Survey, 4200 University Drive, Anchorage, AK 99508, USA.

D. Dzurisin. David A. Johnston Cascades Volcano Observatory, US Geological Survey, 1300 SE Cardinal Court, Building 10, Suite 100, Vancouver, WA 98683-9589, USA.

¹Corresponding author (e-mail: lu@usgs.gov).

the subsidence associated with the 1993 eruption of Mount Etna, Italy (Massonnet et al., 1995), the technique has become an important geodetic imaging tool for studying volcanoes worldwide (e.g., Amelung et al., 2000; Beauducel et al., 2000; Zebker et al., 2000; Massonnet and Sigmundsson, 2000; Wicks et al., 1998; Pritchard and Simons, 2002; Lu et al., 2003b).

The Aleutian volcanic arc lies north of the convergent boundary where the Pacific Plate is being actively subducted beneath the North American Plate along the North Pacific rim. Volcanism in the Aleutians is intimately related to this subduction process, although the timing and character of individual eruptions are strongly influenced by such factors as magma composition, magma supply rate, and crustal structure. The Aleutian arc contains about 10% of the world's active volcanoes and, during the past 100 years, eruptions have occurred there at an average rate of about 15 per decade (Miller et al., 1998). InSAR has been used to study ground deformation associated with both eruptive and noneruptive activity at more than a dozen Aleutian volcanoes. These investigations include pre-eruption inflation, co-eruption deflation, and post-eruption inflation at Okmok volcano (Lu et al., 1998; 2000a; 2005; Mann et al., 2002); progressive aseismic inflation and a model of the magma plumbing system at Westdahl volcano (Lu et al., 2000c; 2003a); magmatic intrusion at Mount Peulik volcano and its relation to an earthquake swarm 30 km away in 1998 (Lu et al., 2002a); magmatic intrusion at Makushin volcano associated with a small eruption in 1995 (Lu et al., 2002b); complex patterns of transient deformation during and after the 1992–1993 eruption at Seguam volcano (Lu et al., 2003b; Masterlark and Lu, 2004); uplift from 1993 to 1995 at New Trident volcano (Lu et al., 1997); surface subsidence caused by a decrease in pore-fluid pressure in an active hydrothermal system beneath Kiska volcano (Lu et al., 2002c); compaction of young pyroclastic flow deposits at Augustine volcano (Lu et al., 2003b); and the absence of deformation associated with recent eruptions at Shishaldin, Pavlof, Cleveland, and Korovin volcanoes (Lu et al., 2003b). All of these studies utilized C-band (wavelength $\lambda = 5.66$ cm) SAR images acquired by the European Space Agency ERS-1 or ERS-2 satellites.

Loss of interferometric coherence is the major obstacle to applying InSAR at Aleutian volcanoes (Lu and Freymueller, 1998; Lu et al., 2002b). SAR returns must be coherent to derive useful information from interferograms. At Aleutian volcanoes, processes that reduce interferometric coherence include snow-ice melting and accumulation, freezing-thawing of surface material, and erosion-deposition of volcanic ash. Vegetation cover is another important factor. Sparsely vegetated lava flows and rocky surfaces maintain coherence at C-band for periods of 3 years or more, even where covered by grass (Lu and Freymueller, 1998; Lu et al., 2002b). Pyroclastic deposits are coherent at C-band for more than 1 year, and densely vegetated lava, rocks, and alluvium typically maintain coherence throughout a single summer (Lu et al., 2002b). At Hawaiian volcanoes, Rosen et al. (1996) showed that interferometric coherence from L-band data ($\lambda = 24$ cm) is much greater than

that from C-band data because of greater penetration of longer wavelength L-band signals.

Akutan volcano and the 1996 seismic swarm

Akutan volcano, situated in the west-central part of Akutan Island in the eastern Aleutian volcanic arc, is a composite stratovolcano with a circular summit caldera about 2 km across. An active cinder cone, about 1 km wide at its base, is located in the northeast quadrant of the caldera (Newhall and Dzurisin, 1988; Miller et al., 1998) (**Figure 1**). Several fumarolic areas are present in the south and southwest parts of the caldera. A breach in the north caldera rim channels volcanic flows from intracaldera vents in that direction. Lava flows, pyroclastic flows, fall, and other types of volcanic deposits cover much of the west portion of the island, including Akutan volcano. The east half of the island, on the other hand, consists mainly of older, relatively loose deposits (tephra and ash) and undifferentiated volcanic rocks (Richter et al., 1998; Miller et al., 1998). In general, vegetation is denser on the east half of the island than on the west half, as shown by the Landsat-7 image in **Figure 1**. Vegetation at higher elevations consists mainly of sparsely distributed short grass, and lush tundra predominates at lower elevations.

Akutan is one of the most active volcanoes in the Aleutian arc. More than 27 eruptive episodes have been noted in the last two centuries (Miller et al., 1998). Most of the reported eruptions included small to moderate explosions from the active intracaldera cone. The most recent eruptive activity was a series of small steam and ash emissions between March and May 1992.

Akutan Island was shaken by an intense swarm of volcano-tectonic earthquakes that peaked between 11 and 16 March 1996 and then slowly declined over the next several months. More than 3000 earthquakes were located using four temporary seismic stations on the island (**Figure 1**). The estimated cumulative seismic moment of the swarm is 2.7×10^{18} N-m, which is approximately equivalent to a single magnitude 6.0 earthquake (Lu et al., 2000b). In the summer of 1996, scientists from the Alaska Volcano Observatory (AVO) discovered fresh ground cracks that extended discontinuously from the area near Lava Point at the northwest end of the island to the southeast tip a few kilometres south of Akutan Village (**Figure 1**). The cracks broke snowfields, and their sides showed little evidence of erosion, suggesting they had formed recently, almost surely during the March 1996 swarm. The most extensive cracks occurred in a zone roughly 500 m wide and 3 km long between Lava Point and the summit of Akutan volcano. Local graben structures with vertical displacements of 30–80 cm suggest that the cracks formed in response to extensional stress perpendicular to the cracks. The cracks on the east side of the island are only a few centimetres wide and apparently represent reactivation of mapped normal faults (Richter et al., 1998).

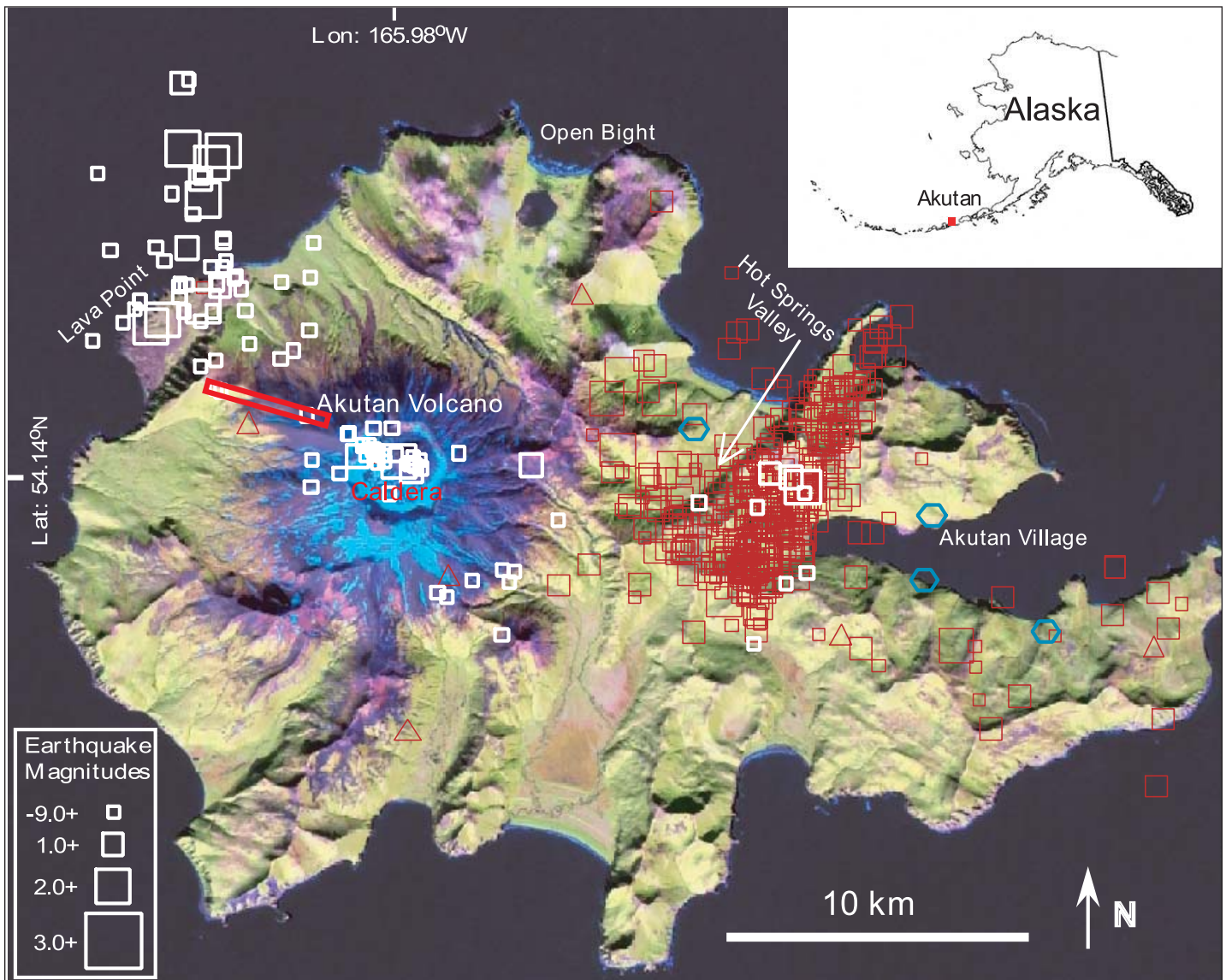


Figure 1. Landsat-7 color-composite image, acquired in August 2002, showing surface characteristics of Akutan Island. Akutan volcano is situated on the western part of the island. The location of Akutan Island along the 2500 km long Aleutian volcanic arc is shown in the inset, upper right. The Landsat-7 image was created by assigning bands 5, 4, and 3 to red, green, and blue, respectively. Bright blue areas represent ice and snow. Sparsely vegetated areas, such as young lava flows and rocky high-alpine areas, are shown in purple. More densely vegetated areas appear as shades of green. Sparsely vegetated alluvium deposits appear pink. Red squares represent earthquakes located using four temporary seismic stations (hexagons) between 18 March and 26 July 1996. The north-northeast trend of the epicenters, roughly perpendicular to the alignment of the four seismic stations, is probably an artifact of poor network geometry. Earthquakes located using both temporary stations and permanent stations (triangles) from 1 August 1996 to 31 December 1998 are represented by white squares. The overall west-northwest trend of these better located events, roughly parallel to mapped normal faults on the island, is real. The lower left inset shows the earthquake magnitude scale. The red rectangle on the northwest flank of Akutan volcano represents a zone of ground cracks and graben structures that formed during the March 1996 earthquake swarm.

InSAR observations of ground surface deformation associated with the March 1996 seismic swarm were first reported by Lu et al. (2000b). Ten ERS-1 and ERS-2 SAR images were used to produce six interferograms, which showed that the west half of Akutan Island, including Akutan volcano, was uplifted about 60 cm sometime between June 1995 and October 1996, presumably during the March 1996 swarm (Lu et al., 2000b). Interferometric coherence at C-band was lost for most of the east half of the island, except for a few small

patches where fringe patterns suggest subsidence along an axis trending west-northwest between Lava Point and the southeast tip of the island.

In this study, we produced 34 interferograms from 44 SAR images acquired during 1992–2002 by the C-band ERS-1 and ERS-2 satellites and the L-band JERS-1 satellite. We used the interferograms to systematically analyze surface deformation before, during, and after the 1996 seismic swarm. We also compared the degree to which interferometric coherence was

maintained at L-band and C-band. Lastly, we explored several alternative numerical models that fit the observed ground deformation.

InSAR deformation and coherence observations

We used the two-pass InSAR approach (e.g., Massonnet and Feigl, 1998; Rosen et al., 2000) to produce 34 deformation interferograms with reasonably good coherence. The image acquisition times and associated imaging parameters are shown in **Table 1**. The DEM used to produce the interferograms is the 1 arc-second (about 30 m posting) shuttle radar topography mission (SRTM) DEM, which has a relative vertical accuracy of better than 10 m and an absolute vertical accuracy of better than 16 m (Farr and Kobrick, 2000; SRTM spatial metadata

dataset available from <http://www.metrokc.gov/gis/sdc/raster/elevation/ShuttleRadarTopographyMissionSpatialMetadata.htm>). Based on the known viewing geometries, DEM errors of this magnitude would result in no more than 1 cm of line-of-sight error in the interferograms (Massonnet and Feigl, 1998).

During the 1996 seismic swarm

Three deformation interferograms that bracket the March 1996 swarm are shown in **Figure 2**. They were produced from C-band ERS images acquired along two different orbital tracks. The interferogram in **Figure 2a** spans the period from 20 August 1993 to 7 October 1996, and the interferogram in **Figure 2b** spans the period from 4 June 1995 to 9 July 1997. In both cases, the radar look angle at the image center is about 21.6°. The interferogram in **Figure 2c** covers the time interval from 1 August 1993 to 18 September 1996, with a radar look

Table 1. SAR images used for this study.

Orbit 1 No.	Date 1	Orbit 2 No.	Date 2	B_n (m)	Look angle (°)	Figure No.
110967	1993-08-20	207670	1996-10-07	4	21.6	2a
120329	1995-06-04	211177	1997-06-09	58	21.6	2b
110695	1993-08-01	207398	1996-09-18	35	24.5	2c
314840	1994-10-28	329338	1997-06-22	340	39.0	3, 6a
104683	1992-06-07	110695	1993-08-01	22	24.5	5
104683	1992-06-07	111697	1993-10-10	160	24.5	5
105184	1992-07-12	110194	1993-06-27	17	24.5	5
105685	1992-08-16	110194	1993-06-27	77	24.5	5
106186	1992-09-20	111196	1993-09-05	57	24.5	5
106186	1992-09-20	111697	1993-10-10	8	24.5	5
106687	1992-10-25	111196	1993-09-05	24	24.5	5
106687	1992-10-25	111697	1993-10-10	41	24.5	5
111468	1993-09-24	122333	1995-10-22	186	21.6	5
111969	1993-10-29	202660	1995-10-23	150	21.6	5
206668	1996-07-29	211177	1997-06-09	280	21.6	5
206668	1996-07-29	217690	1998-09-07	173	21.6	5
206668	1996-07-29	223201	1999-09-27	91	21.6	5
207398	1996-09-18	222428	1999-08-04	240	24.5	5
207398	1996-09-18	228440	2000-09-27	131	24.5	5
207670	1996-10-07	211177	1997-06-09	205	21.6	5
207670	1996-10-07	213181	1997-10-27	91	21.6	5
208171	1996-11-11	222700	1999-08-23	100	21.6	5
211177	1997-06-09	217690	1998-09-07	107	21.6	5
216688	1998-06-29	228211	2000-09-11	98	21.6	5
217690	1998-09-07	223201	1999-09-27	264	21.6	5
221927	1999-06-30	227939	2000-08-23	1	24.5	5
222199	1999-07-19	228712	2000-10-16	146	21.6	5
222428	1999-08-04	227939	2000-08-23	35	24.5	5
222428	1999-08-04	228440	2000-09-27	109	24.5	5
222428	1999-08-04	228941	2000-11-01	125	24.5	5
223201	1999-09-27	227710	2000-08-07	187	21.6	5
223430	1999-10-13	238460	2002-08-28	139	24.5	5
227710	2000-08-07	238231	2002-08-12	52	21.6	5
233450	2001-09-12	237458	2002-06-19	215	24.5	5

Note: Dates are image acquisition times given as year-month-day. Orbit numbers include the satellite identification (1, ERS-1; 2, ERS-2; 3, JERS-1) and the orbit on which the images were acquired. The same track number applies to both images in an InSAR pair. B_n , component of interferogram baseline that is perpendicular to the radar look angle at the image center.

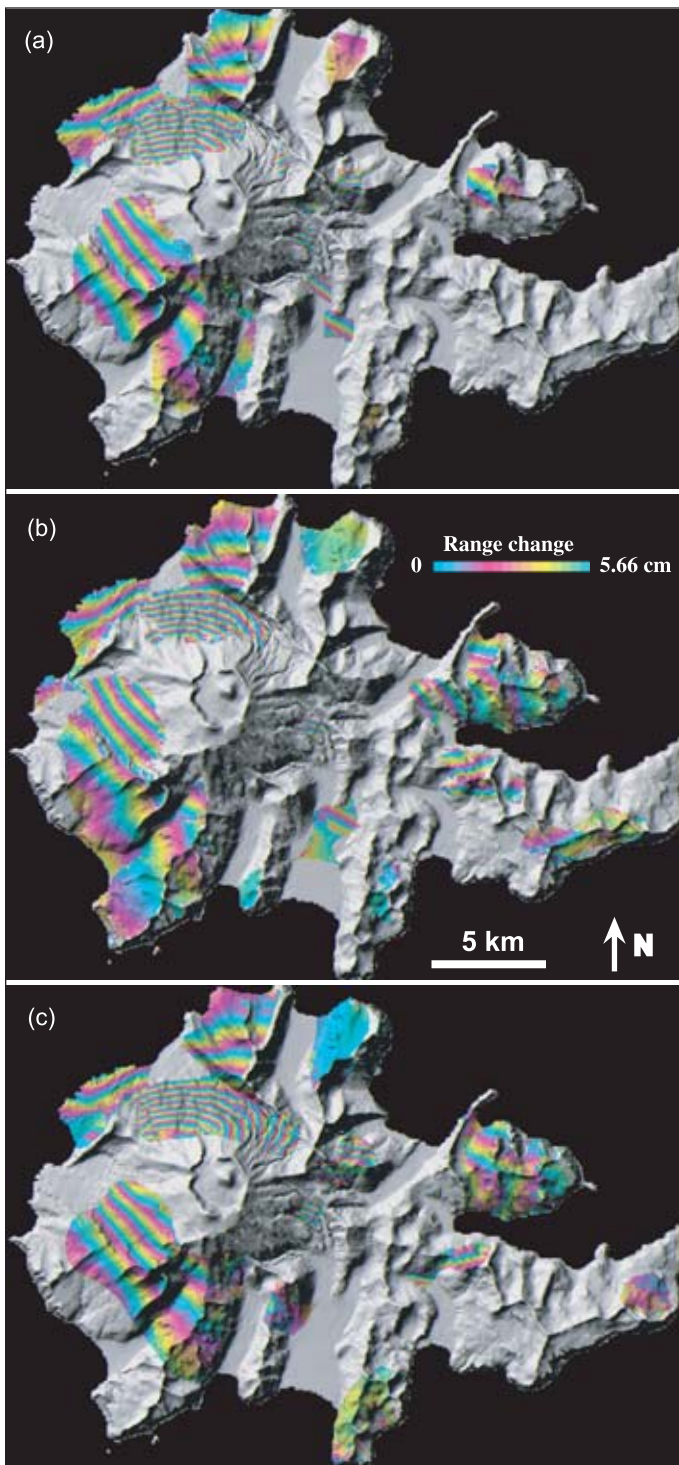


Figure 2. Deformation interferogram of Akutan Island, constructed from C-band ERS-1/2 SAR images, for the periods (a) 20 August 1993 to 7 October 1996, (b) 4 June 1995 to 9 June 1997, and (c) 1 August 1993 to 18 September 1996. Each fringe (full color cycle) represents a 5.66 cm range change in the satellite look direction. Areas that lack interferometric coherence are uncolored.

angle of about 24.5° at the image center. The three interferograms have different baselines and were produced from six independent images (Table 1). All show essentially

the same fringe pattern. Therefore, the observed fringes are not artifacts of orbital errors, topographic errors, or atmospheric delay anomalies but represent ground deformation that must have occurred during the period of overlap in the three interferograms, i.e., between June 1995 and September 1996. The concentric fringe pattern in the western part of the island indicates a maximum decrease in range of about 60 cm (mostly surface uplift owing to the relatively steep look angle of the ERS radars). Interferometric coherence is much worse on the east half of the island, which is covered by relatively loose material and denser vegetation. Still, a few isolated patches of ground in this area maintain coherence. The fringe patterns in these patches suggest subsidence of the eastern part of the island along an axis that trends approximately east–west, similar to the long axis of the island.

An L-band JERS-1 deformation interferogram that spans the time interval from 28 October 1994 to 22 June 1997 is shown in Figure 3a. The accuracy of the satellite position vectors provided in JERS-1 metadata is much poorer than that for ERS-1 and ERS-2 (Massmann, 1995). Therefore, baseline refinement is required for JERS-1 interferogram processing. We refined the baseline (i.e., estimated the vector difference between the two satellite positions from which the images were acquired) by using known elevations from the DEM and applying a least-squares approach (Rosen et al., 1996). In this way, we determined the horizontal and vertical components of the baseline and the rate of change of those components across the interferogram. Based on the ERS interferograms (Figure 2), most of Akutan Island deformed during the 1996 seismic swarm. Therefore, we could not use any portion of the island to refine the baseline. Instead, we used Akutan's neighbor to the east, Akun Island, for this purpose (Figure 3a). Assuming that any deformation of Akun was negligible, we extracted the terrain heights from the DEM and used them to refine the baseline (Rosen et al., 1996).

Comparing the L-band JERS-1 interferogram (Figure 3a) with the C-band ERS interferograms (Figure 2), we can make the following observations:

- (1) Interferometric coherence is significantly higher at L-band than at C-band over similar time intervals. At Akutan, the most coherent interferograms come from SAR images acquired in August or September during arctic summers, when seasonal snow and ice cover is minimal. Even though one of the JERS-1 SAR images was acquired on 28 October 1994, after the island was covered by seasonal snow, the JERS-1 interferogram has much higher coherence than the ERS interferograms (Figure 2). Interferometric coherence studies at other volcanoes (Rosen et al., 1996; Fujiwara et al., 1998) also showed that coherence at L-band is far superior to that at C-band, particularly in heavily vegetated terrain.
- (2) Both the ERS and JERS-1 interferograms show that the western part of the island was uplifted about 60 cm during the 1996 seismic swarm. The JERS-1 interferogram, in addition, shows localized subsidence on

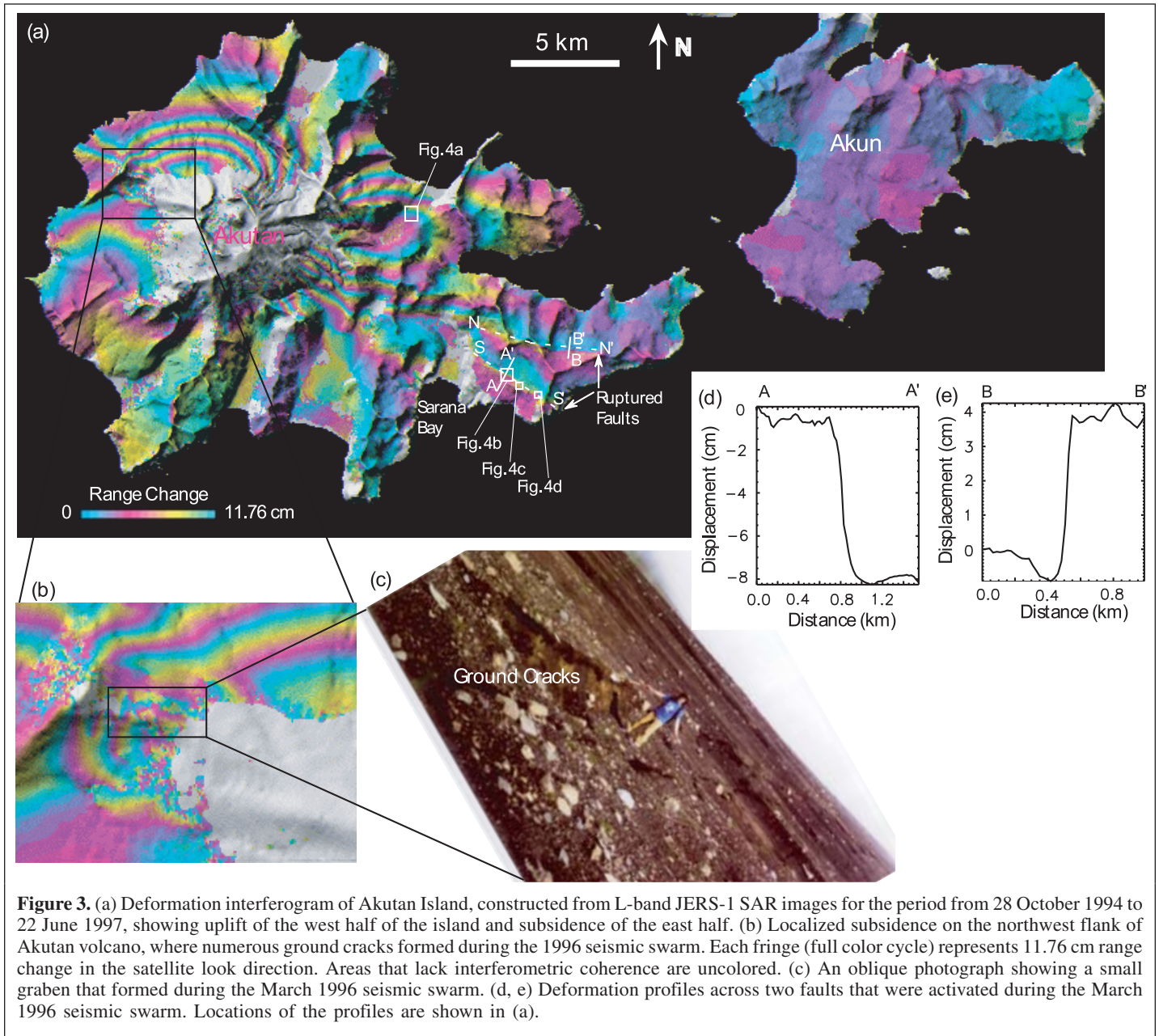


Figure 3. (a) Deformation interferogram of Akutan Island, constructed from L-band JERS-1 SAR images for the period from 28 October 1994 to 22 June 1997, showing uplift of the west half of the island and subsidence of the east half. (b) Localized subsidence on the northwest flank of Akutan volcano, where numerous ground cracks formed during the 1996 seismic swarm. Each fringe (full color cycle) represents 11.76 cm range change in the satellite look direction. Areas that lack interferometric coherence are uncolored. (c) An oblique photograph showing a small graben that formed during the March 1996 seismic swarm. (d, e) Deformation profiles across two faults that were activated during the March 1996 seismic swarm. Locations of the profiles are shown in (a).

the northwest flank of Akutan volcano (**Figure 3b**), in the zone of intense ground cracking associated with the swarm (**Figure 1**). This is consistent with field observations of local graben structures in the zone with vertical displacements of 30–80 cm, which suggest extension and downfaulting (**Figure 3c**). The subsidence is not observable in the ERS interferograms because of loss of interferometric coherence. Wholesale uplift of the volcanic edifice, combined with localized ground cracking and graben formation, has been attributed to magma accumulation and intrusion at other volcanoes (Rubin, 1992).

(3) In the eastern portion of Akutan Island, the JERS-1 interferogram reveals a broad pattern of subsidence

comparable in magnitude to the uplift in the western portion. The subsidence is centered near Hot Springs Valley (**Figures 1** and **4a**), where there are numerous thermal springs (Motyka and Nye, 1988) and where most of the March 1996 earthquakes were located (**Figure 1**). Gas bubbles were observed emerging from springs in the valley during the swarm. The proximity of the area of maximum subsidence, thermal springs, and earthquake epicenters suggest that subsidence reflects depressurization of the hydrothermal system as a result of the swarm. A dense carpet of grass on the valley floor caused interferometric coherence at C-band to be lost in most of this area (**Figures 2** and **4a**).

- (4) The JERS-1 interferogram reveals displacement on two normal faults, N–N' and S–S' over the southeast side of the island (**Figure 3a**). These faults are Holocene normal faults but were rejuvenated in response to tumescence of the volcano in March 1996 (Richter et al., 1998). Ground breakage of several centimetres was observed on the fault N–N' during a field survey in July 1996 (Richter et al., 1998). The fault S–S' was not visited in 1996, and fresh ground breakage was not observed, but the fault scarp was mapped from air photographs (Richter et al., 1998). The fault S–S' was visited in another field survey

conducted in June 2003. The fault scarp can be followed easily both from the air and from the ground. The fault extends to the southeast across the sea cliff, where a phase jump in the interferogram is observable over the southeast end of fault S–S' (**Figure 3a**). The eastern half of the island is covered mainly by loose alluvium and relatively thick vegetation, resulting in loss of coherence in the C-band ERS interferograms. However, portions of faults that cannot be readily identified in the field because they are obscured by erosion or vegetation (**Figures 4c** and **4d**) can be traced in the JERS-1

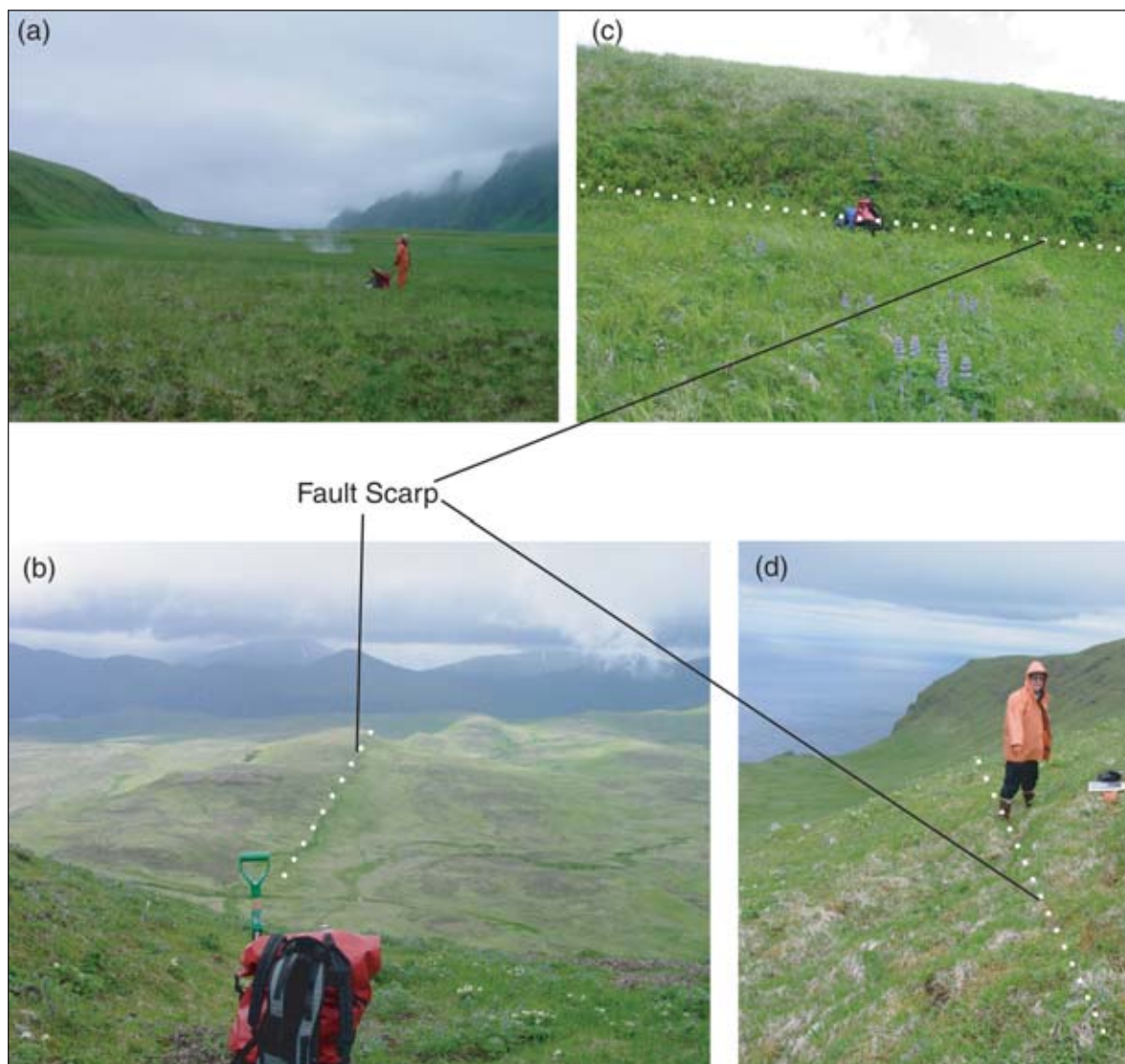


Figure 4. Oblique photographs taken in July 2003 by J.A. Power, showing fault scarps and vegetation on the eastern part of Akutan Island. Approximate locations of the photographs are shown in **Figure 3a**. Interferometric coherence is maintained at L-band in these areas, but not at C band. (a) Photograph, taken near Hot Springs Valley, looks approximately to the north, with a person for scale reference. Hot springs extend from this point down north to the beach. (b) Photograph, showing the scarp of fault S–S', looks to the west along the fault that bounds the south side of the graben. The sense of fault motion is left (south) side up and right (north) side down. (c) Photograph, taken near the scarp of fault S–S', looks approximately to the south, with the shovel and red bag for scale. Heavy ferns growing over the fault scarp can obscure ground breakage of the fault as revealed in the JERS-1 interferogram (**Figure 3a**). (d) Photograph, taken near the southeastern end of fault S–S', looks approximately to the east. The ground breakage of the fault as mapped in the JERS-1 interferogram (**Figure 3a**) can be obscured by erosion of loose material.

interferogram (**Figure 3a**). This further demonstrates the usefulness of the L-band interferogram in mapping displacement of faults that could be difficult to measure from the ground because of dense vegetation or erosion.

- (5) To estimate the displacement of the faults identified in the JERS-1 interferogram (**Figure 3a**), the phase image is unwrapped (Costantini, 1998; Wegmuller et al., 2002). Over fault N–N' (**Figure 3a**), a phase jump can be observed that corresponds to a line-of-sight displacement of about 5 cm (**Figure 3e**). Because the interferogram phase values are continuous over the southeastern end of fault N–N', the displacement measurement in **Figure 3e** is unambiguous (i.e., phase jump across the fault is less than 2π). The measured displacement agrees with the observed ground breakage of several centimetres (Richter et al., 1998). The sense of slip along this fault based on field observation is the north side up and the south side down, which is consistent with the measurement from the interferogram (**Figure 3e**). Over fault S–S' (**Figure 3a**), however, the interferometric phase jump across the fault could be ambiguous because the area to the south of the fault is connected to the rest in the interferogram through the fault. The coherent area to the north of Sarana Bay (**Figure 3a**) is disconnected from the southern block of fault S–S' owing to loss of interferometric coherence. As there is no evidence of north–south faulting activity over the area of loss of coherence, we assume that the difference in interferometric phases between the southern block of fault S–S' and the coherent area to the north of Sarana Bay is less than 2π . With this assumption, the phase values over the southern block of fault S–S' can be connected with the rest of the interferogram through phase unwrapping. The deformation profile across fault S–S' is then shown in **Figure 3d**. It can be seen that the displacement on fault S–S' is similar to that on fault N–N'. The field survey done in June 2003 suggests that fault S–S' appears to dip to the north, and the sense of displacement on fault S–S' is the north side down and the south side up. This observation is consistent with the displacement measurement from the interferogram (**Figure 3d**). Based on the displacement measurements revealed in the JERS-1 interferogram and field observations, we suggest that the two normal faults define a graben about 3 km wide and 5 km long on the southeast side of the island (**Figure 3a**).
- (6) The sense of displacement on two faults on the southeast side of the island suggests that the faults were activated in response to extensional stress perpendicular to the faults (**Figures 3d** and **3e**). The same inference can be drawn from the ground cracks and graben structures that formed on the northwest flank of Akutan volcano (**Figures 3b** and **3c**). The orientations of the faults, ground cracks, and graben structures are all about N70°W (**Figure 1**). Theory predicts that the orientations of normal faults and dikes should be parallel to the direction of maximum horizontal compressive stress (i.e.,

perpendicular to the minimum compression direction) (Nakamura, 1977). Near Akutan Island, relative motion of the Pacific and North American plates, as portrayed by the NUVEL-1A–NNR plate kinematic model (DeMets et al., 1994), results in a convergence direction of about N40°W. In the absence of other tectonic influences, this should approximate the direction of maximum horizontal compressive stress. However, Nakamura et al. (1977; 1980) used the orientations of normal faults and dikes as indicators of tectonic stress trajectories in Alaska and concluded that the maximum compressive stress direction is more nearly N60°W–N70°W near Akutan Island. Their result was based on observations not only at Akutan volcano but also at nearby Makushin, Recheshnoi, and Vsevidof volcanoes. In all four cases, the inferred direction of maximum compressive stress is more westerly than the direction of the plate convergence in this part of the arc.

The reason for this discrepancy is not known, but one possibility is that tectonic stress trajectories vary along the arc because of plate segmentation. This idea is supported by geodetic and seismic observations in the region that indicate that the portion of the arc from the Shumagin Islands, offshore the west-central part of the Alaska Peninsula, more than 500 km southwestward beyond Akutan to at least Umnak Island, differs from the adjacent portions in two ways. First, the Shumagin portion has not been the site of a great (magnitude $M > 8$) subduction earthquake at least since 1903, despite a relatively high convergence rate (~ 75 mm/year). This fact led Davies et al. (1981) to coin the term “Shumagin seismic gap” and Jacob (1984) to suggest that the area has high potential for such an event within the next decade. However, no measurable strain was detected by electronic distance measurement (EDM) observations in the Shumagin Islands from 1980 to 1987 (Lisowski et al., 1988) or by global positioning system (GPS) observations from 1987 to 1991 (Larson and Lisowski, 1994). Second, GPS measurements on Unimak Island, 80–170 km northeast of Akutan Island (i.e., between the Shumagin Islands and Umnak Island), likewise detected no strain accumulation due to subduction between 1998 and 2001 (Mann and Freymueller, 2003). As first noted by Lisowski et al. (1988), the absence of convergence-parallel strain strongly suggests that the megathrust is not presently locked beneath this segment of the arc.

In this situation, other tectonic influences assume greater significance and the direction of maximum compressive stress does not necessarily align with the direction of plate convergence. In addition to the four anomalous N60°W–N70°W compressive-stress directions mentioned earlier, Nakamura et al. (1977) noted a much greater departure from the plate convergence direction (N40°W) at nearby Okmok volcano (N60°E). Regarding this apparent discrepancy in their results, Nakamura et al. (p. 107) wrote “The scatter in trends of roughly radial normal faults is so large that some make a right angle with each other...All these features are more or less suggestive

that the magnitude of two horizontal principal stress axes are rather close and that the maximum principal stress is vertical, at least near the summit region.” We take this as additional evidence that plate convergence does not play a dominant role in determining the direction of maximum compressive stress at Akutan Island, presumably because the megathrust is not currently locked along this segment of the arc as it appears to be on either side. As a result, compressive stress directions are more variable in the creeping segment and local stresses imposed by magmatic processes have greater sway.

The preferred azimuth of magma intrusion and any associated graben structures is along (or perpendicular to) the direction of the greatest (or least) compressive stress (Anderson, 1936; Delaney et al., 1986). At Akutan, correspondence between the average strike of ground breaks in March 1996 (N70°W) and the direction of maximum compressive stress (N60°–70°W) inferred by Nakamura et al. (1977) suggests that magma intrusion and normal faulting contributed to the deformation pattern produced by the swarm. On the western part of the island, it seems likely that wholesale uplift of Akutan volcano, accompanied by localized faulting and graben subsidence, was caused by magma intrusion. Similar patterns of ground deformation have been attributed to dike intrusions at volcanoes in Iceland and Hawaii, some of which culminated in eruptions (Larsen et al., 1979; Rubin, 1992).

Before the 1996 seismic swarm

Ten interferograms (**Table 1**) were examined for evidence of ground deformation near Akutan volcano prior to the March 1996 swarm. Visual inspection indicates that any deformation during 1992–1995 was subtle (i.e., less than one fringe). Because atmospheric delay anomalies that affect interferograms can swamp small deformation signals (e.g., Zebker et al., 1997), the pre-swarm interferograms were stacked. This procedure, which involves summing a set of spatially registered interferograms, reinforces persistent fringe patterns such as those indicative of ground deformation and suppresses transient sources such as atmospheric delay anomalies. The result is an averaged deformation interferogram, revealing that the northwest flank of Akutan volcano was uplifted about 10 mm/year relative to the southwest flank from 1992 to 1995 (**Figures 5a** and **5f**). The averaged interferogram also shows localized subsidence on the northwest flank in the area where ground cracks formed during the March 1996 swarm (**Figure 5f**). Likewise, the area with the greatest uplift during 1992–1995 coincides with the area of greatest uplift associated with the swarm (**Figures 2** and **3**).

After the 1996 seismic swarm

Twenty interferograms (**Table 1**) were produced using SAR images acquired after the 1996 seismic swarm. By stacking interferograms that span a similar period, we produced averaged interferograms for 1996–1997, 1997–1998, 1998–2000, and 2000–2002 (**Figures 5b–5e**). During 1996–1997, the zone of ground cracks that formed during the March 1996 swarm subsided about 20 mm while the rest of the northwest

flank of Akutan volcano was uplifted a comparable amount (**Figures 5b** and **5f**). Only one interferogram is available for 1997–1998 (**Figure 5c**), so there is no opportunity to suppress any atmospheric anomalies that might be present by stacking. With that qualification, the interferogram suggests an additional ~10 mm uplift of the northwest flank of the volcano with respect to the southwest flank. The deformation patterns for 1998–2000 and 2000–2002 (**Figures 5d** and **5e**) are similar to that for 1992–1995 (**Figure 5a**). We conclude from **Figure 5** that the northwest flank of Akutan volcano was uplifted relative to the southwest flank at rates of 5–20 mm/year both before and after the March 1996 earthquake swarm, whereas the area of March 1996 ground cracks subsided at a rate of a few to ~20 mm/year (**Figure 5f**). Subsidence was most rapid during 1996–1997 and slowed considerably thereafter. We speculate that cooling and degassing of magma intruded beneath Akutan volcano in March 1996 contributed to the observed subsidence.

Modeling of deformation during the 1996 seismic swarm

The complexity of the deformation field revealed by the interferograms in **Figures 2** and **3** makes it difficult to identify a unique model for the deformation sources. We explored a range of possible models using as constraints the asymmetric uplift of Akutan volcano, the geometry of surface fractures on its northwest flank, the orientation of reactivated faults on the eastern part of the island, and the distribution of well-located 1996–2000 earthquake epicenters. We present only one model here that fits the essential features of the deformation field as revealed by the interferograms. For this study, we modeled the 1994–1997 JERS-1 interferogram (**Figure 3**) using elastic dislocation sources (Okada, 1985). The rectangular elastic dislocation source consists of 10 model parameters: two location coordinates for the center of the source (x , y), depth (z), length, width, three components of slip (two in the plane of the dislocation surface and one perpendicular to it), and the strike and dip of the dislocation plane. For volcanic deformation modeling, the slip components in the plane of the dislocation surface are constrained to be zero, which reduces the dislocation source to an expanding or contracting slab. The main assumption in constructing the model is that the deforming medium is a homogeneous, isotropic, elastic half-space. The three-dimensional displacements predicted by the model are converted into line-of-sight displacements (i.e., range changes) by projecting along the satellite look direction, and solutions are sought to minimize the squared misfit between the calculated range changes and the observed range changes from the interferograms.

We first used forward modeling to identify a reasonable set of initial parameters for a particular source. Next, we applied a simulated annealing technique with many iterations and perturbations to find the best-fitting parameters for the source (Press et al., 1992). When no further improvement on the misfit could be achieved, we introduced a second source and repeated the procedure. Then a third source was introduced, and so on,

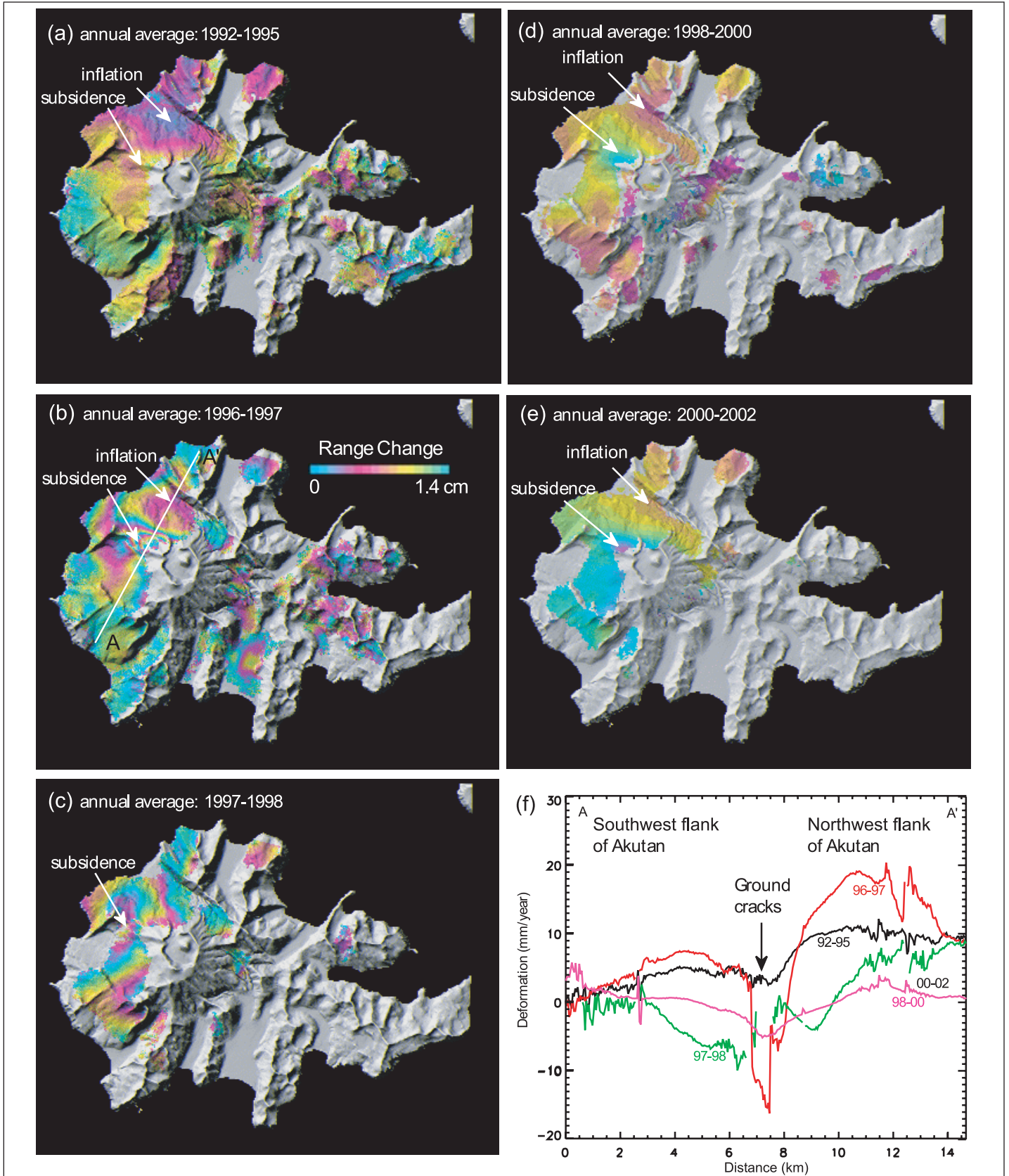


Figure 5. (a–e) Stacked annual average interferograms of Akutan Island constructed from interferograms acquired before and after the 1996 seismic swarm: (a) 1992–1995, (b) 1996–1997, (c) 1997–1998, (d) 1998–2000, and (e) 2000–2002. Each fringe (full color cycle) represents 1.4 cm range change in the satellite look direction. Areas that lack interferometric coherence are uncolored. (f) Surface height changes along profile A–A' across the west flank of Akutan volcano (shown in b).

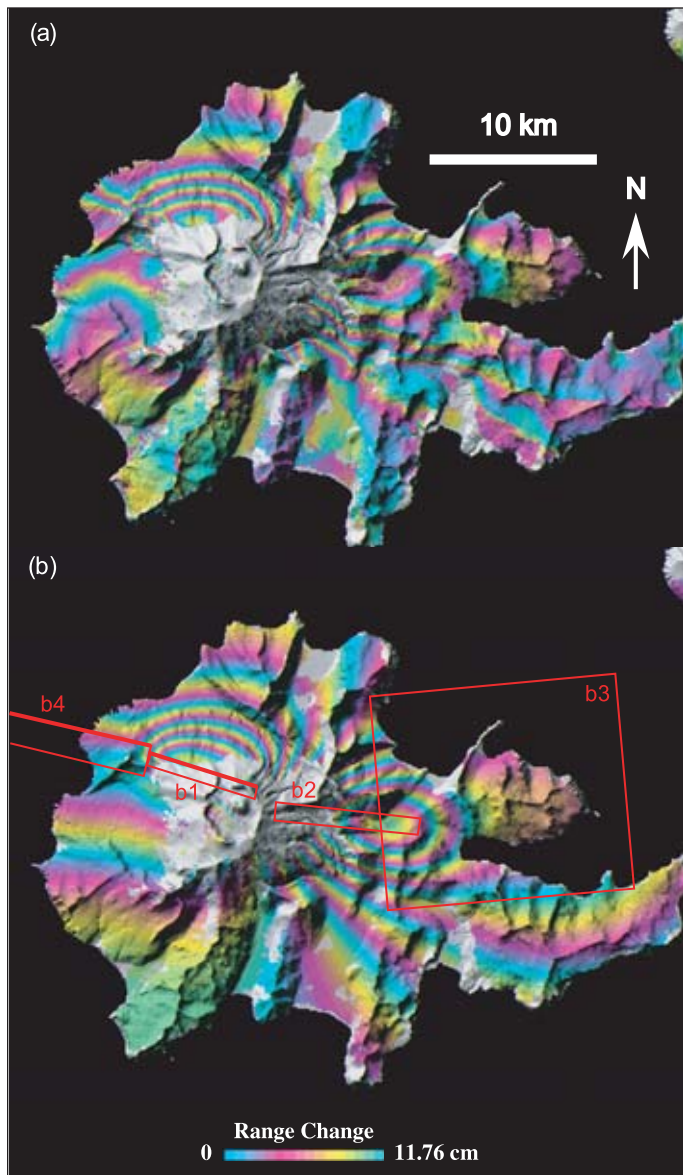


Figure 6. Observed and modeled interferograms of Akutan Island. (a) Observed JERS-1 interferogram. (b) Synthetic interferogram showing the deformation produced by four best-fitting dislocation sources. Rectangles represent the surface projections of the four dislocation planes. The surface projections of the bottom edges of sources b1 and b4 are drawn with thicker lines (sources b2 and b3 are horizontal). Source parameters are shown in **Table 2**. Each fringe (full color cycle) represents 11.76 cm range change in the satellite look direction. Areas that lack interferometric coherence are uncolored.

until the main features of the interferogram were accounted for and no further improvement was apparent.

Figure 6 illustrates a four-source model that fits the observed deformation field reasonably well. The model parameters are listed in **Table 2**. Source b1 is a shallow expanding source that strikes N82°W, dips 75°, and has its top 0.4 km beneath the surface. This source represents an intruding dike that accounts for uplift of the west part of island, including Akutan volcano.

Table 2. Parameters for the best-fitting dislocation model.

	Source 1 (b1)	Source 2 (b2)	Source 3 (b3)	Source 4 (b4)
<i>x</i> coordinate (km)	6.0	11.9	16.1	-0.9
<i>y</i> coordinate (km)	18.4	16.6	21.4	19.5
Depth, <i>z</i> (km)	0.4	3.6	16.5	6.7
Strike	N72°W	N84°W	N115°W	N87°W
Dip (°)	75	0	0	83
Along-strike slip (m)	0	0	0	0
Up-dip slip (m)	0	0	0	0
Tensile slip (m)	1.7	-5.6	-3.9	-4.8
Length (km)	5.1	6.5	11.1	11.0
Width (km)	2.1	0.8	9.7	7.1

Note: Horizontal coordinates (*x*, *y*) are measured with respect to the southwest corner of the area shown in **Figure 6**.

Sources b2 and b3 are contracting sources with horizontal dislocation planes at depths of 3.6 and 16.5 km, respectively. Together, they account for observed subsidence of the eastern part of the island. Their physical meaning is unclear, but depressurization of a hydrothermal system by normal faulting is a reasonable possibility. Source b4 beneath the western part of Akutan Island is also a contracting source, in this case with a steeply dipping dislocation plane and a top at 6.7 km depth. This fourth source accounts for intense ground cracking and graben subsidence on the northwest flank of Akutan volcano (**Figure 6**). It might represent the combined effects of magma withdrawal from depth and surface extension caused by shallow dike intrusion.

Discussion and conclusions

In theory, L-band interferograms are less sensitive to ground deformation than C-band interferograms, because of the longer wavelength of L-band signals. However, comparison of L-band and C-band interferometric coherence at Akutan Island demonstrates that, in practice, L-band is far superior to C-band for studying volcanic surfaces covered with thick vegetation or loose material. Interferograms produced from C-band ERS images that span the March 1996 seismic swarm are coherent mostly on the western part of the island and provide little useful information on the eastern part. On the other hand, an L-band JERS-1 interferogram is coherent and depicts a complex deformation pattern across nearly the entire island. Only the L-band interferogram captures graben subsidence on the northwest flank of Akutan volcano and displacement along reactivated faults on the eastern part of the island. It also reveals fault scarps that are obscured by thick vegetation and therefore difficult to identify from the ground. We conclude that InSAR is a useful tool for measuring deformation of Aleutian volcanoes. Where lava flows predominate, C-band interferograms are better for detecting small deformation signals. Over areas covered by loose material or thick vegetation, however, L-band interferograms are superior. Because more than 70% of the world's active volcanoes are covered by thick vegetation or seasonal snow (Newhall and Dzurisin, 1988), L-band InSAR is

more generally useful for studying volcano deformation worldwide. Therefore, an L-band radar should be the choice of a future InSAR mission on volcano monitoring. For InSAR to become an effective volcano hazards mitigation tool, shorter imaging repeat times (on the order of a few days rather than weeks) and better orbit control (yielding better baselines and thus more useable image pairs, and minimizing artifacts due to baseline errors) are essential.

Combining both L-band JERS-1 and C-band ERS-1/2 InSAR images, we have mapped an uplift of more than 60 cm on the western part of Akutan Island associated with the 1996 seismic swarm. In addition, the JERS-1 interferogram shows subsidence of similar magnitude on the eastern part of the island, plus displacements of a few centimetres along faults reactivated during the swarm. The axis of uplift and subsidence strikes about N70°W, which is roughly parallel to (i) a zone of fresh cracks on the volcano's northwest flank, (ii) normal faults that cut the island, and (iii) the inferred maximum compressive stress direction. The best model that fits the observed deformation suggests the emplacement of a shallow dike along this trend beneath the volcano's northwest flank. Both before and after the swarm, the northwest flank was uplifted 5–20 mm/year relative to the southwest flank, probably by magma intrusion. The zone of fresh cracks on the northwest flank of Akutan volcano subsided approximately 20 mm during 1996–1997 and at lesser rates thereafter, possibly because of cooling and degassing of the magma intrusion.

The ability to map surface deformation at high spatial resolution with InSAR makes it an especially useful tool for studying complex deformation patterns, such as those associated with the March 1996 seismic swarm at Akutan Island. Interferograms presented in this study provide a rare glimpse of surface deformation associated with magma intrusion beneath an island-arc volcano. Such effects are often obscured by subsequent eruptive activity, including syn- and post-eruption deformation that might not be distinguishable from pre-eruption effects. InSAR is capable of characterizing volcano deformation in space and time (the latter to a lesser extent because of current SAR mission constraints), and thus of helping to improve understanding of the eruption cycle at many of the world's volcanoes. Better understanding, in turn, supports improved eruption forecasting and hazards mitigation, which are primary goals of the US Geological Survey Volcano Hazards Program.

Acknowledgements

ERS-1/2 and JERS-1 SAR images are copyright 1991–2002 European Space Agency (ESA) and Japan Aerospace Exploration Agency (JAXA), respectively, and were provided by the Alaska Satellite Facility (ASF) and JAXA. This research was supported by funding from the National Aeronautics and Space Administration (NRA-99-OES-10 RADARSAT-0025-0056) and, in part, by the US Geological Survey contract O3CRCN0001 and the US Geological Survey Land Remote

Sensing Program and Volcano Hazards Program. We thank the ASF and JAXA for their excellent support in providing SAR data on a timely basis, B. Ramachandran, D. Gesch, and three anonymous reviewers for useful and constructive comments and suggestions, and R. Rykhus for assistance with generating **Figure 1**.

References

- Amelung, F., Jonsson, S., Zebker, H., and Segall, P. 2000. Widespread uplift and 'trapdoor' faulting on Galapagos volcanoes observed with radar interferometry. *Nature (London)*, Vol. 407, pp. 993–996.
- Anderson, E.M. 1936. The dynamics of the formation of con-sheets, ring-dikes and cauldron-subsidences. *Proceeding of the Royal Society of Edinburgh*, Vol. 56, pp. 128–157.
- Beauducel, F., Briole, P., and Froger, J.L. 2000. Volcano-wide fringes in ERS satellite radar interferograms of Etna (1992–1998): deformation or tropospheric effect? *Journal of Geophysical Research*, Vol. 105, pp. 16 391 – 16 402.
- Costantini, M. 1998. A novel phase unwrapping method based on network programming. *IEEE Transactions on Geoscience and Remote Sensing*, Vol. 36, pp. 813–821.
- Davies, J., Sykes, L., House, L., and Jacob, K. 1981. Shumagin seismic gap, Alaska Peninsula: history of great earthquakes, tectonic setting, and evidence of high seismic potential. *Journal of Geophysical Research*, Vol. 86, pp. 3821–3855.
- Delaney, P., Pollard, D., Ziony, J., and McKee, E. 1986. Field relations between dikes and joints: emplacement processes and paleostress analysis. *Journal of Geophysical Research*, Vol. 91, pp. 4920–4938.
- DeMets, C., Gordon, R.G., Argus, D.F., and Stein, S. 1994. Effect of recent revisions to the geomagnetic reversal time scale on estimates of current plate motions. *Geophysical Research Letters*, Vol. 21, pp. 2191–2194.
- Dvorak, J., and Dzurisin, D. 1997. Volcano geodesy: the search for magma reservoirs and the formation of eruptive vents. *Review of Geophysics*, Vol. 35, pp. 343–384.
- Dzurisin, D. 2003. A comprehensive approach to monitoring volcano deformation as a window on eruption cycle. *Review of Geophysics*, Vol. 41, 10.1029/2001RG000107.
- Farr, T.G., and Kobrick, M. 2000. Shuttle Radar Topography Mission produces a wealth of data. *Eos*, Vol. 81, pp. 583–585.
- Fujiwara, S., Rosen, P., Tobita, M., and Murakami, M. 1998. Crustal deformation measurements using repeat-pass JERS-1 synthetic aperture radar interferometry near the Izu Peninsula, Japan. *Journal of Geophysical Research*, Vol. 103, pp. 2411–2426.
- Jacob, K.H. 1984. Estimates of long-term probabilities for future great earthquakes in the Aleutians. *Geophysical Research Letters*, Vol. 11, pp. 295–298.
- Larsen, G., Gronvold, K., and Thorarinsson, S. 1979. Volcanic eruption through a geothermal borehole at Namafjall, Iceland. *Nature (London)*, Vol. 278, pp. 707–710.
- Larson, K.M., and Lisowski, M. 1994. Strain accumulation in the Shumagin Islands: results of initial GPS measurements. *Geophysical Research Letters*, Vol. 21, No. 6, pp. 489–492.

- Lisowski, M., Savage, J.C., Prescott, W.H., and Gross, W.K. 1988. Absence of strain accumulation in the Shumagin seismic gap, Alaska, 1980–1987. *Journal of Geophysical Research*, Vol. 93, No. B7, pp. 7909–7922.
- Lu, Z., and Freymueller, J. 1998. Synthetic aperture radar interferometry coherence analysis over Katmai volcano group, Alaska. *Journal of Geophysical Research*, Vol. 103, pp. 29 887 – 29 894.
- Lu, Z., Fatland, R., Wyss, M., Li, S., Eichelberger, J., Dean, K., and Freymueller, J. 1997. Deformation of New Trident volcano measured by ERS-1 SAR interferometry, Katmai National Park, Alaska. *Geophysical Research Letters*, Vol. 24, No. 6, pp. 695–698.
- Lu, Z., Mann, D., and Freymueller, J. 1998. Satellite radar interferometry measures deformation at Okmok Volcano. *Eos*, Vol. 79, No. 39, pp. 461–468.
- Lu, Z., Mann, D., Freymueller, J., and Meyer, D. 2000a. Synthetic aperture radar interferometry of Okmok volcano, Alaska: radar observations. *Journal of Geophysical Research*, Vol. 105, pp. 10 791 – 10 806.
- Lu, Z., Wicks, C., Power, J., and Dzurisin, D. 2000b. Ground deformation associated with the March 1996 earthquake swarm at Akutan volcano, Alaska, revealed by satellite radar interferometry. *Journal of Geophysical Research*, Vol. 105, pp. 21 483 – 21 496.
- Lu, Z., Wicks, C., Dzurisin, D., Thatcher, W., Freymueller, J.T., McNutt, S.R., and Mann, D. 2000c. Aseismic inflation of Westdahl volcano, Alaska, revealed by satellite radar interferometry. *Geophysical Research Letters*, Vol. 27, No. 11, pp. 1567–1570.
- Lu, Z., Wicks, C., Dzurisin, D., Power, J., Moran, S., and Thatcher, W. 2002a. Magmatic inflation at a dormant stratovolcano: 1996–98 activity at Mount Peulik volcano, Alaska, revealed by satellite radar interferometry. *Journal of Geophysical Research*, Vol. 107, doi:10.1029/2001JB0009471.
- Lu, Z., Power, J., McConnell, V., Wicks, C., and Dzurisin, D. 2002b. Pre-eruptive inflation and surface interferometric coherence characteristics revealed by satellite radar interferometry at Makushin volcano, Alaska: 1993–2000. *Journal of Geophysical Research*, Vol. 107, No. B11, pp. 2266–2279, doi:10.1029/2001JB000970.
- Lu, Z., Masterlark, T., Power, J., Dzurisin, D., and Wicks, C. 2002c. Subsidence at Kiska volcano, western Aleutians, detected by satellite radar interferometry. *Geophysical Research Letters*, Vol. 29, No. 18, 1855, doi:10.1029/2002GL014948.
- Lu, Z., Masterlark, T., Dzurisin, D., Rykhus, R., and Wicks, C. 2003a. Magma supply dynamics at Westdahl volcano, Alaska, modeled from satellite radar interferometry. *Journal of Geophysical Research*, Vol. 108, No. B7, 2354, doi:10.1029/2002JB002311.
- Lu, Z., Wicks, C., Dzurisin, D., Power, J., Thatcher, W., and Masterlark, T. 2003b. Interferometric synthetic aperture radar studies of Alaska volcanoes. *Earth Observation Magazine (EOM)*, Vol. 12, No. 3, pp. 8–18.
- Lu, Z., Masterlark, T., and Dzurisin, D. 2005. Interferometric synthetic aperture radar (InSAR) study of Okmok volcano, Alaska, 1992–2003: magma supply dynamics and post-emplacement lava flow deformation. *Journal of Geophysical Research*, Vol. 110, doi:10.1029/2004JB003148. In press.
- Mann, D., and Freymueller, J. 2003. Volcanic and tectonic deformation of Unimak Island in the Aleutian Arc, Alaska. *Journal of Geophysical Research*, Vol. 108, doi:10.1029/2002JB001925.
- Mann, D., Freymueller, J., and Lu, Z. 2002. Deformation associated with the 1997 eruption of Okmok volcano, Alaska. *Journal of Geophysical Research*, Vol. 107, No. B4, doi:10.1029/2001JB000163.
- Massmann, F.H. 1995. *Information for ERS PRL/PRC users*. GeoForschungsZentrum Potsdam, Technical Note.
- Massonnet, D., and Feigl, K. 1998. Radar interferometry and its application to changes in the Earth's surface. *Review of Geophysics*, Vol. 36, pp. 441–500.
- Massonnet, D., and Sigmundsson, F. 2000. Remote sensing of volcanic deformation by radar interferometry from various satellites. In *Remote sensing of active volcanism*. Edited by P.J. Mouginiis-Mark, J.A. Crisp, and J.H. Fink. American Geophysical Union, Washington, D.C. pp. 207–221.
- Massonnet, D., Briole, P., and Arnaud, A. 1995. Deflation of Mount Etna monitored by spaceborne radar interferometry. *Nature (London)*, Vol. 375, pp. 567–570.
- Masterlark, T., and Lu, Z. 2004. Transient volcano deformation sources imaged with InSAR: application to Seguam island. *Journal of Geophysical Research*, Vol. 109, B01401, doi:10.1029/2003JB002568.
- Miller, T.P., McGimsey, R.G., Richter, D.H., Riehle, J.R., Nye, C.J., Yount, M.E., and Dumoulin, J.A. 1998. *Catalog of the historically active volcanoes of Alaska*. US Geological Survey, Open-file Report 98-582.
- Motyka, R., and Nye, C. 1988. *A geological, geochemical, and geophysical survey of the geothermal resources at Hot Springs Bay Valley, Akutan Island, Alaska*. Alaska Division of Geological and Geophysical Surveys, Report of Investigations 88-3.
- Nakamura, K. 1977. Volcanoes as possible indicators of tectonic stress orientation — principle and proposal. *Journal of Volcanology and Geothermal Research*, Vol. 2, pp. 1–16.
- Nakamura, K., Jacob, K.H., and Davies, J.N. 1977. Volcanoes as possible indicators of tectonic stress orientation — Aleutians and Alaska. *Pure and Applied Geophysics (PAGEOPH)*, Vol. 115, pp. 87–112.
- Nakamura, K., Plafker, G., Jacob, K.H., and Davies, J.N. 1980. A tectonic stress trajectory map of Alaska using information from volcanoes and faults. *Bulletin of the Earthquake Research Institute*, Vol. 55, pp. 89–100.
- Newhall, C.G., and Dzurisin, D. 1988. *Historical unrest at large calderas of the world*. US Geological Survey, Bulletin 1855. 1108 pp.
- Okada, Y. 1985. Surface deformation due to shear and tensile faults in a half-space. *Bulletin of the Seismological Society of America*, Vol. 75, No. 4, pp. 1135–1154.
- Press, W., Teukolsky, S., Vetterling, W., and Flannery, B. 1992. *Numerical recipes in C, the art of scientific computing*. Cambridge University Press, New York. 994 pp.
- Pritchard, M., and Simons, M. 2002. A satellite geodetic survey of large-scale deformation of volcanic centers in the central Andes. *Nature (London)*, Vol. 418, pp. 167–171.
- Richter, D.H., Waythomas, C.F., McGimsey, R.G., and Stelling, P.L. 1998. *Geologic map of Akutan Island, Alaska*. US Geological Survey, Open-file Report 98-135. 22 pp.
- Rosen, P., Hensley, S., Zebker, H., Webb, F., and Fielding, E.J. 1996. Surface deformation and coherence measurements of Kilauea volcano, Hawaii, from SIR-C radar interferometry. *Journal of Geophysical Research*, Vol. 101, pp. 23 109 – 23 125.
- Rosen, P.A., Hensley, S., Joughin, I.R., Li, F.K., Madsen, S.N., Rodriguez, E., and Goldstein, R.M. 2000. Synthetic aperture radar interferometry. *Proceedings of the IEEE*, Vol. 88, No. 3, pp. 333–382.

- Rubin, A.M. 1992. Dike-induced faulting and graben subsidence in the volcanic rift zones. *Journal of Geophysical Research*, Vol. 97, pp. 1839–1858.
- Wegmuller, U., Werner, C., Strozzi, T., and Wiesmann A. 2002. Processing strategies for phase unwrapping for INSAR applications. In *EUSAR 2002, Proceedings of the 4th European Conference on Synthetic Aperture Radar*, 4–6 June 2002, Cologne, Germany. VDE Verlag GMBH, Berlin.
- Wicks, C., Thatcher, W., and Dzurisin, D. 1998. Migration of fluids beneath Yellowstone Caldera inferred from satellite radar interferometry. *Science (Washington, D.C.)*, Vol. 282, pp. 458–462.
- Zebker, H., Rosen, P., and Hensley, S. 1997. Atmospheric effects in interferometric synthetic aperture radar surface deformation and topographic maps. *Journal of Geophysical Research*, Vol. 102, pp. 7547–7563.
- Zebker, H., Amelung, F., and Jonsson, S. 2000. Remote sensing of volcano surface and internal processing using radar interferometry. In *Remote sensing of active volcanism*. Edited by P.J. Mougins-Mark, J.A. Crisp, and J.H. Fink. American Geophysical Union, Washington, D.C. pp. 179–205.